Structural Mechanism for STI-571 Inhibition of Abelson Tyrosine Kinase

Thomas Schindler,[1] William Bornmann,[3] Patricia Pellicena,[4] W. Todd Miller,[4] Bayard Clarkson,[3] John Kuriyan[1,2]*

The inadvertent activation of the Abelson tyrosine kinase (Abl) causes chronic myelogenous leukemia (CML). A small-molecule inhibitor of Abl (STI-571) is effective in the treatment of CML. We report the crystal structure of the catalytic domain of Abl, complexed to a variant of STI-571. Critical to the binding of STI-571 is the adoption by the kinase of an inactive conformation, in which a centrally located "activation loop" is not phosphorylated. The conformation of this loop is distinct from that in active protein kinases, as well as in the inactive form of the closely related Src kinases. These results suggest that compounds that exploit the distinctive inactivation mechanisms of individual protein kinases can achieve both high affinity and high specificity.

A hallmark of CML is a reciprocal chromosomal translocation involving the long arms of chromosomes 9 and 22 (*1*). This somatic mutation fuses a segment of the *bcr* gene, from chromosome 9, to a region upstream of the second exon of the *c-abl* gene from chromosome 22. *c-abl* encodes a nonreceptor tyrosine kinase that has tightly controlled activity in normal cells. In contrast, Bcr-Abl fusion proteins have constitutive catalytic activity, despite the fact that the amino acid sequence of the Abl segment of Bcr-Abl is identical to that of c-Abl. The reason for the elevated catalytic activity of the Bcr-Abl fusion protein is poorly understood, but it is clear that this activity of the kinase domain is necessary for the ability of the Bcr-Abl protein to transform cells and cause malignancy.

A series of inhibitors, based on the 2-phenylaminopyrimidine class of pharmacophores, have been identified that have exceptionally high affinity and specificity for Abl (*2*). The most potent of these, STI-571 (Fig. 1A, formerly referred to as Novartis compound CGP 57148), has been successfully tested in clinical trials as a therapeutic agent for CML. The compound has led to complete hematological response in 96% of patients treated for more than 4 weeks at a dose level of 300 mg, and is well tolerated (*3*).

Protein kinase inhibitors typically bind at the highly conserved nucleotide-binding pocket of the catalytic domain. Specific inhibitors of protein kinases take advantage of limited sequence variation surrounding the ATP-binding site [e.g. (*4, 5*)], as well as conformational differences between inactive and active forms of kinases (*6*). STI-571 has a high affinity for Abl kinase, while being essentially inactive against Ser/Thr-kinases and most of the tyrosine kinases [notable exceptions are two related receptor tyrosine kinases, the platelet-derived growth factor (PDGF) receptor (*7*) and c-kit (*8*)].

To determine how STI-571 achieves this high specificity, we solved the crystal structure of a variant of STI-571 (Fig. 1A) bound to the catalytic domain of Abl at 2.4 Å resolution (Fig. 1B) (*9, 10*). There is strong electron density in difference electron density maps for the STI-571 variant, which occupies the site where the adenine base of ATP is normally bound (Fig. 2A). When compared to the pyrazolo-pyrimidine inhibitor PP1 bound to the Src-kinase Hck (*11*) STI-571 extends much further into the catalytic domain, and its pyridinyl group is inserted underneath helix αC in the NH_2-terminal lobe of the kinase. The compound is kinked at the secondary amino group, and it straddles the highly conserved NH_2-terminal region of the "activation loop" (Fig. 1B). The inhibitor that we have crystallized differs from STI-571 in that it lacks a piperazinyl group that is attached to the phenyl-ring of STI-571 (Fig. 1A). The piperazinyl group increases the solubility of the parent compound, but does not alter target discrimination significantly (*2*); it is likely to lie along a solvent accessible and partially hydrophobic groove on the back of the kinase that is left unfilled by the STI-571 variant.

The activation loop controls catalytic activity in most kinases by switching between different states in a phosphorylation-dependent manner (*12*). In fully active kinases, the loop is stabilized in an open conformation by phosphorylation on serine, threonine or tyrosine residues within the loop, and in this conformation a β-strand in the loop provides a platform for substrate binding. Three highly conserved residues in the NH_2-terminal region of this loop (an Asp-Phe-Gly motif, residues 381 to 383 in Abl) are thereby held in a conformation that is appropriate for metal ion ligation by the aspartic side chain. This "active" conformation of the loop is very similar in all known structures of active kinases. There is, however, great diversity in the conformations of this loop in inactive protein kinases, in which the loop often occludes substrate binding. Additionally, crankshaft-like displacements in the NH_2-terminal region of the loop change the conformation of the Asp-Phe-Gly triad, thereby inhibiting the ability of the kinase to bind ATP productively (*13*).

Tyr^{393} in the activation loop is the major site of phosphorylation in Abl, but the form of Abl that we have crystallized is not phosphorylated. The activation loop is folded into the active site of the kinase, and Tyr^{393} forms a hydrogen bond with Asp^{363}, a strictly conserved side chain that is crucial for catalysis (Fig. 1C). Tyr^{393} is presented to the active site by a small antiparallel β-sheet that is formed by a portion of the activation loop. Interestingly, the activation loop mimics the binding mode of substrates, as was also found in the insulin receptor tyrosine kinase (IRK, Fig. 1D) (*14*).

Is the structure of the activation loop in Abl a natural conformation of this region of the protein, or is it induced by the binding of STI-571? Except for the NH_2-terminal anchor region, STI-571 does not interact directly with the activation loop (Fig. 1C). The striking similarity between the conformation of the activation loop and the manner in which peptide substrates bind to tyrosine kinases suggests that the loop is in a natural auto-inhibitory conformation (Fig. 1D). Comparison of the catalytic domains of Abl and inactive IRK shows that the central part of the activation loop in both kinases occludes the mouth of the catalytic domain and interferes with the productive binding of peptide substrates in a similar manner (Fig. 1D). Although Tyr^{393} is positioned exactly as in a substrate peptide, the kinase domain is not in a conformation that is competent for phosphate transfer to the tyrosine, since the inward movement of the activation loop is coupled to displacement of the Asp-Phe-Gly motif away from the active conformation in both kinases [Asp^{381} points away from the active site (Fig. 1C)]. Despite these similarities, STI-571 is inactive against IRK, most likely because a side chain which forms a critical contact with the inhibitor (Thr^{315}, see below) at the periphery of the nucleotide binding site of Abl is not conserved in IRK.

[1]Laboratories of Molecular Biophysics and [2]Howard Hughes Medical Institute, The Rockefeller University, 1230 York Avenue, New York, NY 10021, USA. [3]Memorial Sloan-Kettering Cancer Center, 1275 York Avenue, New York, NY 10021, USA. [4]Department of Physiology and Biophysics, School of Medicine, State University of New York at Stony Brook, Stony Brook, NY 11794, USA.

*To whom correspondence should be addressed. E-mail: kuriyan@rockefeller.edu

In contrast to its interactions with the activation loop, where STI-571 is likely to recognize a natural conformation of the Abl molecule, its interactions with the NH_2-terminal lobe of the kinase appear to involve an induced fit mechanism. The loop between the first two β-strands, which normally binds the phosphate groups of ATP, folds down to increase surface complementarity with the drug. This flap is held in place by a water-mediated hydrogen bond between Tyr^{253}, a residue in the NH_2-terminal lobe of the kinase that immediately follows the β1-β2 loop, and the side chain of Asn^{322}. A similar conformation for this loop was found in the fibroblast growth factor receptor tyrosine kinase domain bound to a high-affinity oxindole-based inhibitor (*4*). This loop is known to be an extremely mobile element in protein kinases, and the induced fit is likely to be readily accommodated.

The inhibitor also interacts with the kinase through hydrogen bonds, some of which confer specificity (Fig. 2). The nitrogen in the pyridinyl ring that is attached to the pyrimidine moiety accepts a hydrogen bond from the amide of Met^{318}, which is normally hydrogen bonded to the nitrogen N1 in ATP. The side chain of Thr^{315} forms a hydrogen bond with the secondary amino group in the inhibitor. This residue is replaced by a methionine in many protein kinases, e.g., IRK. Methionine cannot form this hydrogen bond, and its side chain would also interfere with the binding of the phenyl-moiety of STI-571. The presence of Thr^{315} is therefore a key requirement for the ability of this class of compounds to inhibit Abl.

An ion-pair between two strictly conserved side chains (Lys^{271} and Glu^{286} in Abl) is a characteristic feature of the active conformations of protein kinases. This ion pair is disrupted in the inactive conformations of many protein kinases, such as the Src and cyclin-dependent kinases, but not in the STI-571 complex of Abl. Instead, a network of hydrogen bonds involving the side chain of residues Lys^{271} and Glu^{286}, as well as the main chain of Asp^{381}, the acid amide group of the inhibitor and two water molecules further stabilizes binding (Fig. 2).

There are a number of van der Waals interactions between protein residues Tyr^{253}, Leu^{370}, Phe^{382}, Met^{290}, and Ile^{313}, and the aromatic rings of the inhibitor, resulting in an exceptional level of surface complementarity. The snug fit hardly allows for any modification on either the inhibitor or the kinase domain without compromising binding affinity. Conversely, alterations in the sequences of other protein kinases in the regions that make up the binding site, such as the replacement of Thr^{315} by methionine, would interfere with binding.

The most interesting aspect of the interaction between STI-571 and the Abl kinase is that specificity is also achieved at a level beyond simple sequence requirements. The residues that contact STI-571 in Abl kinase are either identical in the Src-family tyrosine kinases, or are substituted conservatively. Nevertheless, the phenylamino-pyrimidines are virtually inactive against the Src-family tyrosine kinases (*2*). The residues that are not identical in Abl and the Src kinases are also variant in the c-kit and PDGF receptor tyrosine kinases, which are the only other kinases sensitive to inhibition by STI-571. These alterations in sequence therefore do not seem to account for lack of sensitivity of the Src-kinases for inhibition by STI-571 and its derivatives.

Like Abl, the Src-family tyrosine kinases are also inactivated by an inward movement of the activation loop when it is not phosphorylated (*11, 15*). Although the loop blocks substrate binding in inactive Src kinases, it does not do so by mimicking a substrate, and its conformation is quite different from that seen in Abl (Fig. 3). The inactive conformation of the activation loop in Src kinases is coupled to a particular "swung-out" conformation of helix αC, which is not observed in our Abl structure. The most important consequence of this for the binding of STI-571 is that the conformation of the NH_2-terminal anchor of the activation loop (containing the conserved Asp-Phe-Gly motif) is quite different in the inactive Src kinase and Abl structures. The conformation of this region in the Src kinases would block the binding of STI-571 (Fig. 3).

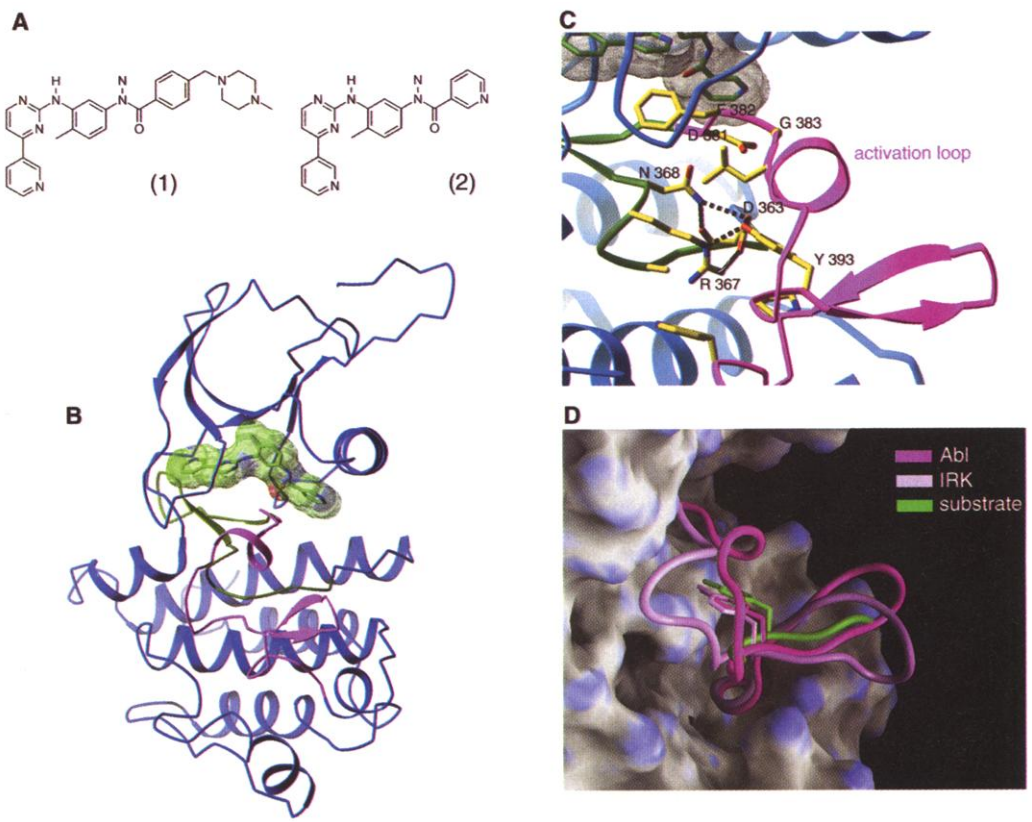

Fig. 1. Crystal structure of the catalytic domain of Abelson tyrosine kinase complexed with a variant of STI-571. (**A**) Structural formula of the Abl inhibitor STI-571 (panel 1) and the variant (panel 2) used in this crystallographic study. (**B**) Ribbon representation of the three-dimensional structure of Abl kinase domain in complex with the STI-571 variant shown in (A). The molecular surface of the inhibitor is shown. A central conserved region of the kinase, the catalytic segment, is shown in green and the activation loop in magenta. (**C**) Ribbon representation of the activation loop of Abl. The polypeptide backbone of the activation loop is shown in magenta. Hydrogen-bonding interaction are depicted by dashed lines. Tyr^{393} is the site of phosphorylation within the activation loop. (**D**) The polypeptide region in the vicinity of the Tyr^{393} is shown. Superimposed is the peptide substrate (green), as seen in the structure of insulin receptor tyrosine kinase (IRK) complexed with peptide substrate (*14*), and the activation loop of IRK in the inactive form (light pink) (*32*). The figure was generated by superimposing the catalytic segments of the two kinases.

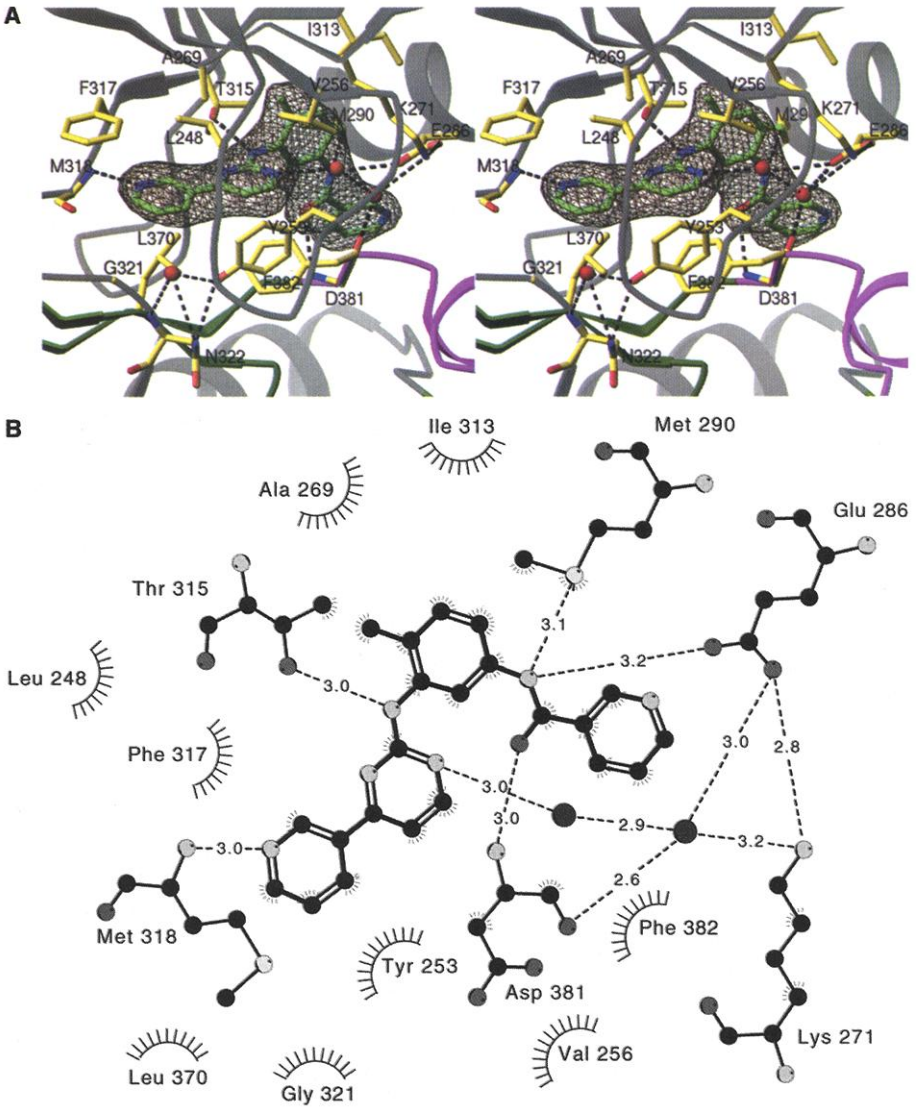

Fig. 2. Mode of binding of the STI-571 variant binding to Abl tyrosine kinase. (**A**) Stereoview of the nucleotide-binding pocket of Abl. The side chains of residues that interact with the inhibitor are shown, as are main-chain atoms and water molecules participating in hydrogen bonds. Carbon atoms are yellow (protein) and green (inhibitor), oxygen atoms are red, nitrogen atoms are blue, and sulfur atoms are green. Hydrogen bonds are shown as dashed lines. Electron density, calculated using ($|F_o| - |F_c|$) coefficients, is shown for the inhibitor only (contoured at 2.5 σ), and was computed using phases from a model obtained after simulated annealing with the inhibitor omitted. (**B**) Schematic drawing of Abl kinase interactions with the STI-571 variant, generated by LIGPLOT (*33*). Residues forming van-der-Waals interactions are indicated, those participating in hydrogen bonds are shown in a ball-and-stick representation. Hydrogen bonds are depicted as dotted lines with the donor-acceptor distance given in Å.

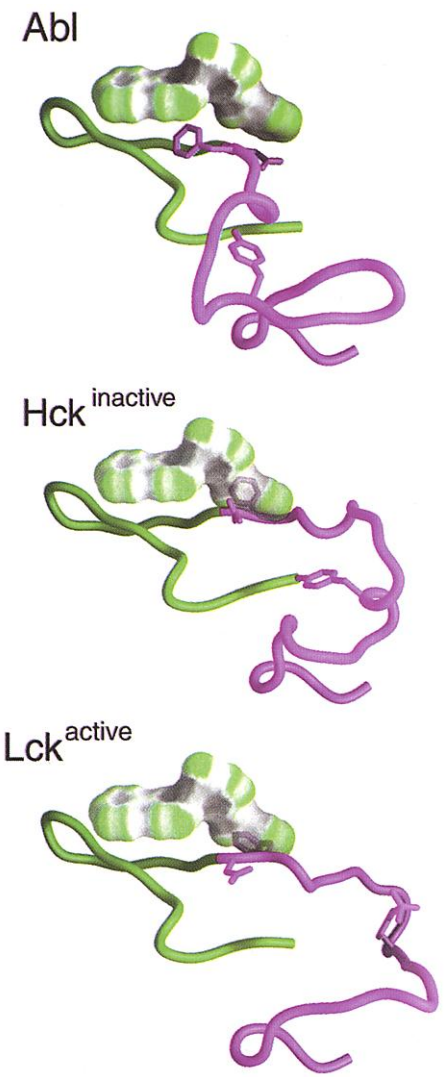

Fig. 3. STI-571 exploits the unique conformation of the activation loop in the down-regulated form of Abl. Conformation of the activation loops of Abl and the Src kinases Lck (active) (*16*) and Hck (inactive) (*11*). Also shown is a space-filling model of the Abl-specific inhibitor. The figure was generated by superimposing the catalytic segments of the displayed kinases. The structures of Lck and Hck are representative for the active and the inactive state of Src-family tyrosine kinases, respectively. The active form of Abl is expected to resemble that of Lck. The activation loop is magenta, the catalytic segment green. The conserved side chains of the Asp-Phe-Gly motif and the tyrosine residue in the activation loop are shown in a ball-and-stick representation.

Phosphorylation of Tyr^{393} in Abl would destabilize the closed conformation of the activation loop because of electrostatic repulsion between the phosphoryl group and the side chain of Asp^{363}. We expect that phosphorylation on Tyr^{393} would stabilize the activation loop in the open conformation seen in active protein kinases, such as the Src kinase Lck (*16*) (this appears to be a structurally conserved feature of activated protein kinases). Interestingly, the conformation of the NH_2-terminal anchor of the activation loop in active protein kinases is also inconsistent with the binding of STI-571 (Fig. 3). We therefore predict that the phosphorylated form of Abl will be less susceptible to inhibition by STI-571.

We tested this by comparing the catalytic activity of the unphosphorylated and phosphorylated forms of the Abl kinase domain in the presence of different concentrations of STI-571 (Fig. 4) (*17*). Because Abl is slow to autophosphorylate, we used catalytic amounts of the Src kinase Hck to generate the phosphorylated Abl kinase domain. Hck phosphorylates the kinase domain of Abl specifically at Tyr^{393} in the activation loop (*17*). Activation of c-Abl by Src kinases plays a role in the cellular response to PDGF (*18*) and Hck has been implicated in the Bcr-Abl–induced transformation of cells (*19*).

We found that the activity of unphosphorylated Abl was essentially ablated at an STI-571 concentration of 0.5 μM, whereas Abl treated with Hck retained more than 50% of its initial activity under these conditions (Fig. 4). Even at a 10-fold higher concentration of STI-571 the Hck-treated Abl retained 30% activity. The inhibition constant, K_i, of STI-571 for the unphos-

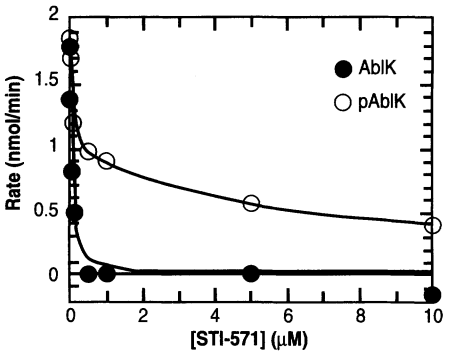

Fig. 4. STI-571 preferentially inhibits the unphosphorylated form of the kinase domain of Abl. Dose response of phosphorylated and unphosphorylated Abl. The kinase activity measured in a continuous spectrophotometric assay is plotted as a function of concentration of STI-571 (*17*). Abl kinase was phosphorylated in the activation loop by pre-incubation with Hck. The reaction rates are corrected for the rate of a control reaction in the absence of Abl kinase. The amount of Hck used did not give a significant signal in the spectrophotometric assay.

phorylated form of Abl was 37 ± 6 nM. The dose-response curve of the phosphorylated form is complex. It can be analyzed by assuming that inhibition occurs in two steps, one with a K_i value of 43 ± 2 nM, which is virtually identical to the K_i obtained for the unphosphorylated form, and another with a much higher K_i of 7 ± 0.2 μM. The biphasic inhibition suggests that the phosphorylation of Abl by Hck did not go to completion, with the low K_i component reflecting inhibition of a remaining population of unphosphorylated kinase molecules.

Interestingly, the catalytic activity of the Abl kinase domain was not increased significantly by phosphorylation in the activation loop (Fig. 4). The inactivation of Abl relies on interactions between the catalytic domain and the SH3 domain of Abl (which is lacking in the construct used here) (*20*–*22*). The unphosphorylated full-length Abl protein is indeed activated upon autophosphorylation (*23, 24*). Presumably, the activation loop of the isolated Abl kinase domain is flexible and can adopt the active conformation without requiring the additional stabilization provided by phosphorylation.

In summary, we have shown that although STI-571 targets the relatively well conserved nucleotide-binding pocket of Abl, it can still achieve high specificity by recognizing a distinctive inactive conformation of the activation loop of Abl. The ability of the catalytic domains of protein kinases to adopt characteristic inactive conformations is proving to be a hallmark of these proteins. That STI-571 takes advantage of this feature of its target is encouraging news for the further development of specific protein kinase inhibitors.

References and Notes

1. C. L. Sawyers, *N. Engl. J. Med.* **340**, 1330 (1999).
2. J. Zimmermann, E. Buchdunger, H. Mett, T. Meyer, N. B. Lydon, *Bioorg. Med. Chem. Lett.* **7**, 187 (1997).
3. B. J. Druker *et al.*, *Blood* (Suppl.) **94**, 368a (1999) (abstract# 1639 presented at the 41st annual meeting of the American Society of Hematology, New Orleans, LA, 3 to 7 December 1999).
4. M. Mohammadi *et al.*, *Science* **276**, 955 (1997).
5. K. P. Wilson *et al.*, *Chem. Biol.* **4**, 423 (1997).
6. Z. Wang *et al.*, *Structure* **6**, 1117 (1998).
7. B. J. Druker *et al.*, *Nature Med.* **2**, 561 (1996).
8. E. Buchdunger *et al.*, *Proc. Am. Assoc. Cancer Res.* **39**, 559 (1998) (abstract# 3801 presented at the 89th annual meeting of the American Association for Cancer Research, New Orleans, LA, 28 March to 1 April 1998).
9. The gene encoding residues 229 to 515 of murine Abelson tyrosine kinase (numbering corresponding to isoform I) was cloned into pFastbac HTa (Gibco BRL), which allows the protein to be expressed fused to a cleavable hexa-histidine-tag. The murine sequence is identical to that of human c-Abl in this region, except for the replacement of Asn to Ser at position 336 in murine Abl. Recombinant baculoviral DNA was obtained from this construct via the Bac-to-bac system (Gibco-BRL). Insect cells (Sf9) grown in suspension were infected with the recombinant baculovirus. After further growth for 48 hours, cells were collected by centrifugation and stored at −80°C. Typically, cell paste corresponding to 4 liters of growth volume was thawed, resuspended, and lysed by sonication. The lysate was clarified by high-speed centrifugation. Abl was purified using anion exchange (macroprep high Q, Bio-Rad) and subsequent affinity chromatography (Ni-NTA Superflow, Qiagen). Tobacco Etch Virus protease was used to cleave Abl kinase from the hexahistidine fusion tag. Before the protein was concentrated, the STI-571-variant [synthesized and purified as described (*2*), dissolved in dimethyl sulfoxide] was added in a threefold molar excess. The inhibitor-protein complex was further purified over a Superdex 75 gel filtration column (HiLoad 16/60) in 20 mM tris-HCl (pH 8.0), 100 mM NaCl, and 3 mM dithiothreitol. Abl kinase used for enzymatic analysis was purified accordingly, except that no inhibitor was added before gel filtration. The peak fractions were concentrated to 30 mg/ml and used for crystallization or kinase assays. Because of the cloning strategy, the protein carries an extension of six amino acid residues [GAMDPS (*25*)] at its NH_2-terminus, so that it comprises 293 amino acids in total.
10. Crystallization of inhibitor-protein complex was carried out by the hanging-drop vapor diffusion technique. We mixed 1 μl of protein-inhibitor complex with an equal volume of reservoir solution consisting of 25% (w/v) polyethylene glycol 4 K, 100 mM mes-NaOH (pH 6.2), and 0.2 M $MgCl_2$. Orthorhombic single crystals grew in about a week at 4°C (space group *F222* with a = 110.7 Å, b = 146.1 Å, c = 152.8 Å, two molecules of Abl kinase-inhibitor complex in the asymmetric unit). Crystals were harvested into a stabilizing solution of 28% (w/v) polyethylene glycol 4 K, 100 mM mes-NaOH (pH 6.2), and 0.2 M $MgCl_2$, and were subsequently cryoprotected in stabilizing solution plus 15% (v/v) ethylene glycol before freezing in liquid nitrogen–cooled liquid propane. Data were collected to 2.4 Å resolution at beamline X25 of the National Synchrotron Light Source (Brookhaven, NY) on a Brandeis B4 charge-coupled device detector (λ = 0.9393 Å). Data processing and reduction were carried out with the HKL package (*26*). X-ray data comprised 24,122 unique reflections derived from 221,636 observations in the 99 to 2.4 Å resolution range with an R_{merge} of 6.8% (21.6 % in the 2.49 to 2.40 Å shell). The diffraction data were 98.7% complete (90.6% in the 2.49 to 2.40 Å shell). The structure was determined by molecular replacement with the atomic coordinates of the kinase domain of Hck (residues 258–520, Protein Data Bank code 1qcf) as the search model. Subsequent refinement utilizing AMORE (*27*), CNS (*28*), and O (*29*) was straightforward. Bulk solvent correction and overall anisotropic B-factor scaling were applied throughout the refinement process (elements of final anisotropic B-factor tensor applied to data: B_{11} = −7.21 Å^2, B_{22} = −1.99 Å^2, and B_{33} = 9.17 Å^2). Our current model consists of 545 amino acid residues, two inhibitor molecules, and 99 water molecules and is refined to an R value of 23.9% (R_{free} = 26.4%) against all data between 99 to 2.4 Å resolution. All nonglycine residues fall into the allowed or the additionally allowed regions of the Ramachandran plot. The rms deviations from ideal bond length and angles are 0.008 Å and 1.4°, respectively. Neighboring main chain and side chain atoms show rms deviations in B values of 1.5 and 1.8 Å^2, respectively. The electron density map was significantly weaker for one of the two kinase molecules in the asymmetric unit, and all the analysis here relied on the better ordered one. Tight, noncrystallographic restraints were utilized throughout the refinement so that the final rms deviation between the two molecules is 0.05 and 0.04 Å for the NH_2-terminal and the COOH-terminal lobes, respectively (excluding residues 229 to 237, 252, 262, 271, 294, 306, 404, 447, 450, 466, and 491, which were built in different conformations in the two molecules).
11. T. Schindler *et al.*, *Mol. Cell* **3**, 639 (1999).
12. L. N. Johnson, M. E. M. Noble, D. J. Owen, *Cell* **85**, 149 (1996).
13. S. R. Hubbard, M. Mohammadi, J. Schlessinger, *J. Biol. Chem.* **273**, 11987 (1998).
14. S. R. Hubbard, *EMBO J.* **16**, 5572 (1997).
15. W. Xu, A. Doshi, M. Lei, M. J. Eck, S. C. Harrison, *Mol. Cell* **3**, 629 (1999).
16. H. Yamaguchi and W. A. Hendrickson, *Nature* **384**, 484 (1996).
17. We employed a continuous spectrophotometric kinase assay in which the production of adenosine diphosphate is coupled to the oxidation of NADH and measured as a reduction in absorbance at 340 nm (*30*). This assay allowed us to measure the activities of phosphorylated and unphosphorylated Abl in the same experiment. We initiated the assay by adding phosphorylated Abl, collected inhibition data, then generated the unphosphorylated form in situ by adding 0.8 μM glutathione *S*-transferase–Yop (*Yersinia* protein tyrosine phosphatase). Reactions were carried at 30°C in 500 μl of buffer containing 100 mM Tris-HCl (pH 7.5), 10 mM $MgCl_2$, 0.5 mM ATP, 1 mM phosphoenol pyruvate, 0.28 mM NADH, 89 units/ml pyruvate kinase, 124 units/ml lactate dehydrogenase, and 0.5 mM of the peptide substrate AEEEIYGEFEAKKKKG (*25, 31*). The concentration of Abl was 10 nM. In experiments with STI-571, reactions and controls also contained 1% dimethyl sulfoxide. Yop treatment had no effect on the enzymes in the coupled assay. Abl was phosphorylated using hematopoietic cell kinase (Hck) at room temperature for 1 hour in 50 μl of 100 mM Tris-HCl (pH 7.5), 10 mM ATP, 30 mM $MgCl_2$, 1.3 μM Abl, and 50 nM Hck. Mass spectrometric data (T. Schindler and J. Kuriyan, data not shown) demonstrated that phosphorylation of Abl by Hck resulted in the incorporation of a single phosphoryl-group. Mass spectrometric analysis of peptides released upon protease digestion of Abl by GluC and LysC confirmed that Tyr^{393} in the activation loop was phosphorylated and that the phosphorylation was incomplete.
18. R. Plattner, L. Kadlec, K. A. DeMali, A. Kazlauskas, A. M. Pendergast, *Genes Dev.* **13**, 2400 (2000).
19. J. M. Lionberger, M. B. Wilson, T. E. Smithgall, *J. Biol. Chem.* **275**, 18581 (2000).
20. W. M. Franz, P. Berger, J. Y. J. Wang, *EMBO J.* **8**, 137 (1989).
21. P. Jackson and D. Baltimore, *EMBO J.* **8**, 449 (1989).
22. D. Barila and G. Superti-Furga, *Nature Genet.* **18**, 280 (1998).
23. K. Dorey and G. Superti-Furga, unpublished data.
24. B. Brasher and R. Van Etten, unpublished data.
25. Single-letter abbreviations for the amino acid residues are as follows: A, Ala; C, Cys; D, Asp; E, Glu; F, Phe; G, Gly; H, His; I, Ile; K, Lys; L, Leu; M, Met; N, Asn; P, Pro; Q, Gln; R, Arg; S, Ser; T, Thr; V, Val; W, Trp; and Y, Tyr.

26. Z. Otwinowski and W. Minor, *Methods Enzymol.* **276**, 307 (1997).
27. J. Navaza, *Acta Crystallogr. D* **50**, 157 (1994).
28. A. T. Brünger *et al.*, *Acta Crystallogr. D* **54**, 905 (1998).
29. T. A. Jones, J. Y. Zou, S. W. Cowan, M. Kjeldgaard, *Acta Crystallogr. A* **47**, 110 (1991).
30. S. C. Barker *et al.*, *Biochemistry* **34**, 14843 (1995).
31. Z. Songyang *et al.*, *Nature* **373**, 536 (1995).
32. S. Hubbard, L. Wei, L. Ellis, W. Hendrickson, *Nature* **372**, 746 (1994).
33. A. Wallace, R. Laskowski, J. Thornton, *Protein Eng.* **8**, 127 (1995).
34. We thank H. Viguet, L. Leighton, and N. Rodionova for technical assistance; H. Lewis, D. Jeruzalmi, and X. Chen for assistance with data collection and analysis; M. Huse, E. Vidal, and M. Young for valuable discussions; B. Mayer for kindly providing mouse Abl cDNA; and K. Dorey, G. Superti-Furga, B. Brasher, and R. van Etten for communication of their unpublished results. T.S. acknowledges fellowship support from the Deutsche Forschungsgemeinschaft (Schi 524/1-1) and the Leukemia & Lymphoma Society. Protein coordinates are available from the Protein Data Bank (code 1fpu).

25 May 2000; accepted 25 July 2000

Respiration and Parturition Affected by Conditional Overexpression of the Ca^{2+}-Activated K^+ Channel Subunit, SK3

Chris T. Bond,[1] Rolf Sprengel,[6] John M. Bissonnette,[2] Walter A. Kaufmann,[5] David Pribnow,[3] Torben Neelands,[1] Thorsten Storck,[6] Manfred Baetscher,[4] Jasna Jerecic,[6] James Maylie,[2] Hans-Günther Knaus,[5] Peter H. Seeburg,[6] John P. Adelman[1]*

In excitable cells, small-conductance Ca^{2+}-activated potassium channels (SK channels) are responsible for the slow after-hyperpolarization that often follows an action potential. Three SK channel subunits have been molecularly characterized. The SK3 gene was targeted by homologous recombination for the insertion of a gene switch that permitted experimental regulation of SK3 expression while retaining normal SK3 promoter function. An absence of SK3 did not present overt phenotypic consequences. However, SK3 overexpression induced abnormal respiratory responses to hypoxia and compromised parturition. Both conditions were corrected by silencing the gene. The results implicate SK3 channels as potential therapeutic targets for disorders such as sleep apnea or sudden infant death syndrome and for regulating uterine contractions during labor.

SK channels are potassium-selective, voltage-independent, and activated by increases in the levels of intracellular Ca^{2+}, such as what occurs during an action potential (*1, 2*). We have characterized three mammalian SK subunits (hSK1, rSK2, and rSK3) by molecular cloning. All three form SK channels with similar Ca^{2+} sensitivity and gating kinetics; constitutive association of calmodulin accomplishes Ca^{2+} gating with an intracellular domain of the channel α subunits (*3, 4*). To investigate the physiological role of murine SK3, we site-specifically inserted a tetracycline-based genetic switch into the 5′ untranslated region of the gene so that subunit expression could be abolished by dietary doxycycline (dox) administration without interfering with the normal profile of SK3 expression (Fig. 1) (*5*).

SK3 mRNA levels were examined in brain tissue from wild-type (+/+), heterozygous (+/T), and homozygous (T/T) targeted mice that were without or with dox (0.5 mg/ml, for at least 5 days before being killed) in their drinking water. Total RNA from whole brains was used for Northern blot analysis and reverse transcriptase–polymerase chain reaction (RT-PCR) (Fig. 1). SK3 mRNA was readily detected from animals not treated with dox, but no hybridization signal was detected from dox-treated animals. Multiplex RT-PCR experiments for SK3 and β-actin (for cross-sample comparison), with equivalent amounts of cDNA from each animal, were analyzed during the linear range of amplification. Among wild-type animals, similar amounts of product were detected, and levels were not affected by dox. In heterozygous animals that were not treated with dox, expression from the two alleles was similar. After dox administration, levels derived from the wild-type allele were not significantly altered, but product derived from the targeted allele was reduced to background levels. SK3 mRNA expression in homozygous targeted mice that were not administered dox was approximately three times that for either allele in heterozygous animals. Expression was undetectable after dox administration. To examine SK3 protein levels, we probed Western blots of membrane preparations from mouse brain with an SK3-specific antibody. SK3 protein was detected before but not after dox treatment. SK3 protein levels in the absence of dox were higher in SK3 T/T mice than in wild-type mice (Fig. 1) (*6*). Western blots for SK2 showed similar levels of protein in wild-type, T/T, or T/T with dox brain membrane preparations (*7*).

The regional distribution of SK3 protein in wild-type and SK3 T/T mice was investigated by immunohistochemistry in the brain (*8, 9*). Most immunoreactivity was associated with the neuropil; individual neuronal perikarya were only occasionally stained. The highest expression levels of SK3 protein were observed in the hippocampal formation, striatum, in subsets of neocortical neurons, thalamus, cerebellum, and brain stem. In particular, SK3 protein was detected in various neuronal populations of the medulla oblongata, which are thought to be involved in the processing of respiratory signals, e.g., the reticular formation and solitary tract nuclei (Fig. 2). For all brain regions investigated, the SK3 distribution profile remained unchanged in SK3 T/T mice when compared with wild-type animals. However, the absolute level of SK3 protein expression in SK3 T/T animals was higher. No SK3 immunoreactivity was detected in sections after dox treatment (Fig. 2). Together, these results demonstrate that, in mice homozygous for the conditional SK3 allele, SK3 expression in the brain is increased in relation to the wild type and expression can be abolished by dietary dox administration. The presence of the regulatory cassette in the exon encoding the 5′ untranslated region does not alter the expression pattern of the SK3 gene.

SK3 is the only known SK subunit expressed in skeletal muscle where expression is highly induced by denervation and in primary cultured myotubes (*10*). To examine SK3 function in skeletal muscle from wild-type and SK3 T/T mice, we prepared myotube cultures in the presence or absence of dox (5 μg/ml) in the media (*11*). After 6 days of culture, action potentials recorded from wild-type myotubes showed a prominent af-

[1]Vollum Institute, [2]Department of Obstetrics and Gynecology, [3]Department of Cell and Developmental Biology, [4]Department of Molecular and Medical Genetics, Oregon Health Sciences University, Portland, OR 97201, USA. [5]Institute of Biochemical Pharmacology, University of Innsbruck, A-6020 Innsbruck/Tyrol, Austria. [6]Department of Molecular Neuroscience, Max-Planck-Institute for Medical Research, D-69120 Heidelberg, Germany.

*To whom correspondence should be addressed. E-mail: adelman@ohsu.edu